MCB
Journals.ASM.org

The PTH-Gα_s-Protein Kinase A Cascade Controls αNAC Localization To Regulate Bone Mass

Martin Pellicelli,[a,b] Julie A. Miller,[a,b] Alice Arabian,[a] Claude Gauthier,[a] Omar Akhouayri,[a]* Joy Y. Wu,[c] Henry M. Kronenberg,[d] René St-Arnaud[a,b]

Research Unit, Shriners Hospitals for Children—Canada, Montreal, Quebec, Canada[a]; Department of Human Genetics, McGill University, Montreal, Quebec, Canada[b]; Division of Endocrinology, Stanford University School of Medicine, Stanford, California, USA[c]; Endocrine Unit, Massachusetts General Hospital, Boston, Massachusetts, USA[d]

The binding of PTH to its receptor induces Gα_s-dependent cyclic AMP (cAMP) accumulation to turn on effector kinases, including protein kinase A (PKA). The phenotype of mice with osteoblasts specifically deficient for Gα_s is mimicked by a mutation leading to cytoplasmic retention of the transcriptional coregulator αNAC, suggesting that Gα_s and αNAC form part of a common genetic pathway. We show that treatment of osteoblasts with PTH(1–34) or the PKA-selective activator N^6-benzoyladenosine cAMP (6Bnz-cAMP) leads to translocation of αNAC to the nucleus. αNAC was phosphorylated by PKA at serine 99 *in vitro*. Phospho-S99-αNAC accumulated in osteoblasts exposed to PTH(1–34) or 6Bnz-cAMP but not in treated cells expressing dominant-negative PKA. Nuclear accumulation was abrogated by an S99A mutation but enhanced by a phosphomimetic residue (S99D). Chromatin immunoprecipitation (ChIP) analysis showed that PTH(1–34) or 6Bnz-cAMP treatment leads to accumulation of αNAC at the *Osteocalcin* (*Ocn*) promoter. Altered gene dosages for Gα_s and αNAC in compound heterozygous mice result in reduced bone mass, increased numbers of osteocytes, and enhanced expression of *Sost*. Our results show that αNAC is a substrate of PKA following PTH signaling. This enhances αNAC translocation to the nucleus and leads to its accumulation at target promoters to regulate transcription and affect bone mass.

Continuous secretion of PTH causes bone resorption (1). However, when administered at a low dosage and intermittently, PTH stimulates bone formation to a greater extent and earlier than it activates resorption (2–4). Intermittent PTH treatment causes pleiotropic effects that all contribute to increase osteoblast number (5).

PTH (and PTHrP) binds the G protein-coupled receptor, PTHR1 (6). Binding of the hormone to PTHR1 induces Gα_s-mediated activation of adenylyl cyclase that stimulates cyclic AMP (cAMP) production. A major effector pathway downstream from the accumulation of cAMP is the activation of protein kinase A (PKA), and PKA is a known transducer of PTH-induced signaling (7). While PKA-independent mechanisms involving the Epac family of guanine nucleotide exchange factors have been implicated in the signal transduction properties of cAMP (8), the contribution of these PKA-independent mechanisms in mediating cAMP-induced signaling in response to the PTH-PTHR1 interaction remains unknown (9). Other pathways are also stimulated by the liganded PTHR1 receptor, such as Gα_q-mediated activation of protein kinase C (PKC) (10).

Structure-function analysis of the PTH molecule has established that PTH-stimulated, Gα_s-dependent cAMP production is sufficient for mediating its anabolic effect, but activation of PKC is insufficient (11, 12). To gain further insight into the role of Gα_s in mediating signaling from G protein-coupled receptors, including PTHR1, in osteoblasts, the gene was conditionally deleted in early osteoblast lineage cells (13). Deletion of Gα_s in osteoblasts that express *Osterix* (*Osx*-Cre; G$\alpha_s^{fl/fl}$ ["fl/fl" represents "flox/flox"] mice) leads to reduced bone mass and abnormal persistence of woven bone. Immature, woven bone often displays high numbers of osteocytes within the matrix (14, 15). Consequently, increased expression of the osteocytic differentiation markers *E11* and *Sost* was detected, together with reduced WNT signaling caused by increased expression of the inhibitors of the WNT signal, *Sclerostin* (*Sost*) and *Dickkopf1* (13). Primary calvarial osteoblasts from *Osx*-Cre; G$\alpha_s^{fl/fl}$ mice demonstrated accelerated mineralization when cultured under osteogenic conditions. Another phenotypic manifestation caused by the absence of Gα_s signaling in osteoblasts was reduced expression of the differentiation marker *Osteocalcin* (*Ocn*) (13).

One of the molecules affecting maximal *Ocn* expression is the transcriptional coregulator αNAC (*n*ascent-polypeptide-associated *c*omplex *a*nd *c*oregulator alpha) (16, 17). αNAC shuttles between the cytoplasm and the nucleus, and one of the signals that induce its nuclear accumulation is phosphorylation by integrin-linked kinase (ILK) (18) at residue Ser43 (19). Nuclear αNAC potentiates *Osteocalcin* (*Ocn*) gene transcription by stabilizing the binding of a c-JUN dimer to its AP-1 binding site within the *Ocn* gene promoter (20, 21). It has further been shown that αNAC can specifically bind DNA and that this DNA-binding capacity is required to potentiate AP-1-mediated *Ocn* gene expression in osteoblasts (16). To determine the physiological role of nuclear αNAC, we engineered a knock-in mouse model with a serine-to-alanine mutation at position 43 (S43A). The S43A mutation resulted in a

Received 28 October 2013 **Returned for modification** 19 November 2013
Accepted 13 February 2014
Published ahead of print 18 February 2014
Address correspondence to René St-Arnaud, rst-arnaud@shriners.mcgill.ca.
* Present address: Omar Akhouayri, Laboratoire de Génétique–Neuroendocrinologie et Biotechnologie, Faculté des Sciences Ibn Tofaïl, Kénitra, Morocco.

doi:10.1128/MCB.01434-13

decrease in nuclear αNAC with reduced *Ocn* promoter occupancy, leading to a significant decrease in *Ocn* gene transcription (17). The bones of the S43A mutant mice had a significantly reduced bone volume. There was a predominance of woven-type bone characterized by an increase in the number of osteocytes. Accordingly, the expression of the osteocyte differentiation markers *E11* and *Sost* was increased. Osteoblasts isolated from the calvaria of mutant $\alpha NAC^{S43A/S43A}$ mice mineralized their matrix faster than wild-type cells (17). Thus, inhibition of αNAC nuclear translocation *in vivo* mimics most of the phenotype of mice in which $G\alpha_s$ has been specifically deleted from osteoblasts (13). This suggests the existence of a signaling cascade linking $G\alpha_s$ and αNAC to control osteoblast function.

We report that treatment of osteoblasts with PTH or a PKA-selective cAMP analog leads to translocation of αNAC to the nucleus and increased binding of the coregulator at its cognate site within the *Ocn* promoter. Purified PKA phosphorylates αNAC *in vitro*, and we have identified the PKA phosphoacceptor site within αNAC. Mutation of this residue affects subcellular localization of αNAC and modulates αNAC-mediated transcriptional activation of the *Ocn* gene promoter. Compound $G\alpha_s$; αNAC heterozygotes have a reduced bone mass phenotype, increased numbers of osteocytes, and enhanced expression of osteocytic differentiation markers, confirming that $G\alpha_s$ and αNAC form part of a common genetic pathway. Taken together, our results support the existence of a signaling cascade that initiates with PTH binding to its receptor, activation of $G\alpha_s$ to stimulate cAMP accumulation, and PKA activity, thus sending αNAC to the nucleus to affect target gene transcription and regulate bone mass.

MATERIALS AND METHODS

Cell lines, antibodies, and reagents. The MC3T3-E1 osteoblastic cell line (22) was cultured in minimum essential medium alpha (αMEM) supplemented with 10% fetal bovine serum (PAA Laboratories/GE Healthcare, Piscataway, NJ) and 1 mM L-glutamine (Life Technologies, Burlington, Ontario, Canada). UMR-106 osteosarcoma cells (23) were cultured in Dulbecco's modified Eagle's medium (DMEM) (Life Technologies) with the same supplements. PTH(1–34) (catalog no. H4835) and PTHrP(1–34) (catalog no. H6630) were purchased from Bachem (Torrance, CA), dibutyryl cAMP (D0627) and 8-(4-chlorophenylthio)-2′-*O*-methyladenosine cAMP (8-PCPT-cAMP; catalog no. C8988) were obtained from Sigma-Aldrich, and N^6-benzoyladenosine cAMP (6Bnz-cAMP; catalog no. B009) was from Biolog (Bremen, Germany), while PD98059 was procured through Cell Signaling Technology (Danvers, MA). Anti-αNAC antibodies have been described previously (17, 24). The affinity-purified rabbit polyclonal anti-αNAC-phospho-S99 antibody (pS99), raised against the peptide NH_2-TGVTRVTIRK-phospho-S-KNILFVITKP-COOH, was produced by and purchased from PhosphoSolutions (Aurora, CO). The anti-c-Myc epitope antibody (9E10) was purchased from Origene (Rockville, MD), while anti-FLAG and anti-α-tubulin antibodies were from Sigma-Aldrich. Secondary antibodies (Alexa Fluor 594–goat anti-chicken and Alexa Fluor 488–goat anti-mouse antibodies) were obtained from Life Technologies.

Primary osteoblast isolation. Primary osteoblasts were isolated as described by Bakker and Klein-Nulend (25). Briefly, calvariae of 5-day-old C57BL/6 mice were isolated after sacrifice. Soft tissue was removed and calvariae were washed in phosphate-buffered saline (PBS). Calvariae were incubated in 4 ml of digestion solution (0.0625% trypsin, 0.8 mg/ml collagenase type II [270 U/mg; Life Technologies], 0.025% EDTA in PBS) at 37°C for 20 min. Following digestion, the supernatant containing isolated osteoblasts was transferred, and calvariae were washed with 3 ml of αMEM, which was then combined with the digestion solution together with 700 μl of fetal bovine serum (FBS). Cells were spun, resuspended in complete αMEM, and plated in 6-well plates (fraction 1). The digestion step was repeated three more times to obtain fractions 2 to 4. Cells were kept 3 to 5 days before passaging for experiments. Only fractions 3 and 4, representing more mature osteoblast populations, were used in this study.

Immunofluorescence. Cells (2.0×10^5) were plated on gelatin-coated coverslips in 6-well plates and grown for 24 h prior to overnight starvation in serum-free medium. The cells were then treated with hormones, analogs, or inhibitors in serum-free medium for 4 to 6 h at 37°C. Following treatment, the cells were fixed in 4% paraformaldehyde (PFA) for 30 min at room temperature, followed by permeabilization with 1% Triton X-100 in Tris-buffered saline (TBS) for 10 min. Samples were then washed twice with 0.1% Tween 20 in TBS (TBS-Tween) and blocked using 3% skim milk and 1% horse serum in TBS-Tween for 60 min at room temperature. This was followed by 2 washes with TBS-Tween and immunodetection with chicken anti-αNAC (1:500) or anti-FLAG (1:500) antibodies in TBS, for 60 min at room temperature. Secondary antibodies (Alexa Fluor 594–goat anti-chicken antibodies at 1:500 or Alexa Fluor 488–goat anti-mouse antibodies at 1:200) were diluted in TBS and added for 30 min at room temperature, followed by 3 washes in TBS-Tween. Slides were mounted with Vectashield mounting medium containing DAPI (4′,6-diamidino-2-phenylindole) (Vector Laboratories, Burlingame, CA). For subcellular localization studies, cells were scored as "nuclear" or "cytoplasmic" based on the localization of the αNAC protein in 100 stably infected cells from different microscopic fields, and the results were expressed as percentage of nuclear αNAC localization. Immunofluorescence images were obtained using a Leica DMR fluorescence microscope (Leica Microsystems, Wetzlar, Germany) connected to a digital DP70 camera (Olympus, Center Valley, PA).

Vector cloning, recombinant αNAC production, and *in vitro* kinase assay. The pSI-αNAC-FLAG vector for mammalian expression and $pTYB_2$-αNAC vector for bacterial expression have been described previously (19). Expression vectors for the S99A and S99D αNAC proteins were obtained by mutating the serine TCT codon to GCT or GAC codons, respectively, within pSI-αNAC-FLAG. Recombinant αNAC (rαNAC) was expressed and purified as previously described (19) and quantified using Coomassie brilliant blue staining of SDS-PAGE gels with graded amounts of bovine serum albumin (BSA) as a standard. *In vitro* kinase assays were performed using recombinant PKA catalytic subunit (Millipore, Billerica, MA) diluted at 16 ng/μl in dilution buffer (20 mM MOPS [morpholinepropanesulfonic acid], pH 7.0, 1 mM EDTA, 0.01% Brij-35, 5% glycerol, 0.1% 2-mercaptoethanol, 1 mg/ml BSA). Reaction mixtures included 200 ng (2 μl) of rαNAC or recombinant CREB protein as a positive control (Novus Biologicals, Oakville, Ontario, Canada), 40 ng (2.5 μl) of diluted PKA, 10 μl of ATP (250 μM ATP, 25 mM Mg acetate, 5 μCi [γ-^{32}P]ATP at 3,000 Ci/mmol; PerkinElmer, Waltham, MA), 5.5 μl of water, and 5 μl of 5× reaction buffer (40 mM MOPS, pH 7.0, 1 mM EDTA) in a final volume of 25 μl. Reactions were performed at 30°C for 20 min and stopped by adding 5 μl of 6× Laemmli buffer and heating at 85°C for 5 min. Total samples were resolved by SDS-PAGE on a 12.5% acrylamide gel. Gels were dried, and protein phosphorylation was revealed by autoradiography on X-ray films. Some kinase assays were performed without radioactive ATP and revealed by immunoblotting with anti-pS99 (1:50) and anti-αNAC (1:250) antibodies.

Infection with lentiviral vectors. The wild-type and mutant αNAC cDNAs were subcloned from the pSI backbone into the pLVX-internal ribosome entry site (IRES)-Puro lentiviral expression vector (Clontech Laboratories, Mountain View, CA) using the EcoRI and NotI restriction sites in both vectors. The c-Myc epitope-tagged PKA-dominant-negative (PKAdn) (cAMP-unresponsive mutant of R1α regulatory subunit) expression vector pcDNA3.1-PKAdn was provided by N. O. Dulin (University of Chicago, Chicago, IL) (26). An NheI-BamHI restriction fragment encompassing the PKAdn cDNA and the c-Myc tag was subcloned into pLVX-IRES-Puro between the SpeI and BamHI restriction sites of the pLVX vector. Lentivirus production and cell infection were performed as previously described (27).

IP and IB. MC3T3-E1, UMR-106, or primary osteoblast cells were plated at 1×10^6 cells in 10-cm-diameter plates. Cells were grown for 24 h, starved overnight in serum-free medium, and treated with the indicated doses of PTH(1–34) or 100 μM PKA-specific cAMP analog N^6-benzoyladenosine cAMP (6Bnz-cAMP). For immunoblotting (IB), whole-cell extracts were prepared by washing cells twice with cold PBS and scraping in 400 μl of radioimmunoprecipitation assay (RIPA) buffer (50 mM Tris-HCl, pH 8.0, 150 mM NaCl, 1% [vol/vol] NP-40, 0.5% [wt/vol] deoxycholate, 0.1% [wt/vol] SDS, 5 mM EDTA, 2.5 mM sodium pyrophosphate, 1 mM β-glycerophosphate, 1 mM sodium orthovanadate, and 1 μg/ml leupeptin, 1 μg/ml aprotinin, 1 mM phenylmethylsulfonyl fluoride protease inhibitors). For immunoprecipitation (IP), the cells were collected in IP buffer (20 mM Tris-HCl [pH 7.5], 150 mM NaCl, 1 mM EDTA, 1 mM EGTA, 1% Triton X-100, 2.5 mM sodium pyrophosphate, 1 mM β-glycerophosphate, 1 mM sodium orthovanadate, with protease inhibitors). Extracts were centrifuged at 13,000 × *g* for 10 min at 4°C to pellet debris, and the protein concentration was determined using Bradford assay reagent (Bio-Rad, Hercules, CA).

For straight immunoblotting, an equal volume of 2× Laemmli loading buffer was added to 50 μg of cell extract. For FLAG-IP, 1 to 2 mg of cell extract was incubated with 20 μl of EZview Red anti-FLAG affinity gel (Sigma-Aldrich) for 16 h on a rotating wheel at 4°C in a final volume of 800 μl. The immunocomplexes were washed 4× with 800 μl of cold IP buffer and resuspended in 40 μl of 2× Laemmli loading buffer. Cell extract proteins and immunoprecipitated proteins were denatured for 5 min at 100°C, resolved by SDS-PAGE on 12.5% acrylamide gels, transferred to polyvinylidene difluoride (PVDF) membranes, and immunodetected with anti-pS99 (1:50), anti-αNAC (1:250), anti-Myc epitope (1:5,000), or anti-α-tubulin (1:10,000) antibodies followed by incubation with appropriate secondary antibody. Blots were developed using the ECL enhanced chemiluminescence Western blotting detection reagent according to the manufacturer's instructions (GE Healthcare Bio-Sciences, Baie d'Urfé, Quebec, Canada).

ChIP. Untransfected cells or cells expressing mutant S99A αNAC or PKAdn were fixed for 10 min at room temperature by adding a concentrated formaldehyde solution directly to the culture media to a final concentration of 1%. The cross-linking reaction was stopped by adding 0.125 M glycine for 5 min at room temperature. Fixed cells were washed twice, scraped in cold PBS, and then centrifuged for 5 min at 500 × *g*. To isolate the nuclei, cells were successively resuspended and centrifuged in nucleus-chromatin preparation (NCP) buffer 1 (HEPES, 10 mM pH 6.5; EDTA, 10 mM; EGTA, 0.5 mM; Triton X-100, 0.25% [vol/vol]) and NCP buffer 2 (HEPES, 10 mM, pH 6.5; EDTA, 1 mM; EGTA, 0.5 mM; NaCl, 200 mM). The nuclear pellet was lysed by resuspension in 800 μl of cold RIPA buffer. One hundred micrograms of total nuclear extract was set aside as an input control. The lysate was sonicated with 10 pulses of 10 s using an Ultrasonic dismembrator model 500 (Thermo Fisher Scientific, Waltham, MA). Lysates were cleaned of debris by centrifugation at 13,000 × *g* for 10 min, and the protein concentration was determined using Bradford protein assays. When chromatin immunoprecipitation (ChIP) was performed against endogenous αNAC, 1 to 2 mg of cross-linked proteins was precleared with protein G-streptavidin-agarose beads (GE Healthcare Biosciences) and salmon sperm DNA prior to immunoprecipitation. Following preclearing, anti-αNAC antibody (1:50) was added, and samples were incubated for 16 h at 4°C on a rotating wheel. Protein-DNA complexes were recovered by incubation with 50 μl of protein G-streptavidin-agarose beads for 1 h at 4°C on a rotating wheel. When ChIP was performed against FLAG-tagged αNAC, the sonicated, cross-linked proteins were directly incubated with 20 μl of EZview Red anti-FLAG affinity gel (Sigma-Aldrich) for 16 h at 4°C. Protein-DNA-bead complexes were successively washed four times with RIPA buffer, four times with lithium chloride buffer (100 mM Tris-HCl, pH 8.0, 500 mM LiCl, 1% [vol/vol] NP-40, 1% [wt/vol] deoxycholate), and one time with 100 mM Tris-HCl (pH 8.0). Washed complexes were eluted from beads by heating in 150 μl of 1% SDS, and cross-links were reversed by heating the samples for 4 to 5 h at 65°C. DNA was purified by phenol-chloroform extraction and precipitated using ethanol and glycogen as a carrier. Chromatin from input and ChIP samples was resuspended in Tris-EDTA (TE) and analyzed by real-time PCR. Target *Ocn* promoter was amplified using SYBR green PCR master mix (Life Technologies) with species-specific primers.

Reporter gene transient-transfection assay. UMR-106 cells were transfected with the p1316-luc *Ocn* proximal promoter reporter plasmid (28) and expression vectors for c-JUN in combination with wild-type αNAC or S99A or S99D mutant αNAC as previously described (19). Transfections were conducted in triplicate, and values are reported as mean fold induction ± standard error of the mean (SEM), with luciferase levels measured in cells transfected with the empty expression vectors arbitrarily ascribed a value of 1.

Generation of compound $G\alpha_s^{ob+/-}$; $\alpha NAC^{+/-}$ heterozygous mice. All animal procedures were reviewed and approved by the McGill Institutional Animal Care and Use Committee and followed the guidelines of the Canadian Council on Animal Care. Mice were kept in an environmentally controlled barrier animal facility with a 12-h light/12-h dark cycle and were fed mouse chow and water *ad libitum*. $G\alpha_s^{fl/fl}$ (29), Osx1-GFP::Cre (30), and conventionally targeted αNAC mutant (31) mice have been described previously. To produce Osx1-GFP::Cre; $G\alpha_s^{+/fl}$; $\alpha NAC^{+/-}$ compound heterozygous mice (abbreviated $G\alpha_s^{ob+/-}$; $\alpha NAC^{+/-}$), mice heterozygous for the targeted αNAC allele ($\alpha Nac^{+/-}$) were first crossed with hemizygous Osx1-GFP::Cre mice to obtain Osx-Cre; $\alpha Nac^{+/-}$ mice. These mice were then crossed with $G\alpha_s^{fl/fl}$ mice to obtain all study genotypes in equivalent proportions: $G\alpha_s^{ob+/+}$; $\alpha Nac^{+/+}$, $G\alpha_s^{ob+/-}$; $\alpha Nac^{+/+}$, $G\alpha_s^{ob+/+}$; $\alpha Nac^{+/-}$, and $G\alpha_s^{ob+/-}$; $\alpha Nac^{+/-}$.

Tissue preparation, μCT, and histomorphometry. Eight-week-old male mice were injected with 25 μg of calcein 7 and 2 days prior to sacrifice. Femurs, tibiae, and L4 vertebrae were dissected and immediately fixed in 4% PFA for 24 h at 4°C. Bones were transferred to 70% ethanol and kept at 4°C until analysis. Micro-computed tomography (μCT) was performed using a SkyScan 1172 high-resolution μCT scanner connected to a Hamamatsu 10-megapixel camera. Images were captured at 65 kV, 153 μA, using a detection pixel of 4,84 μm and a 0.5-mm aluminum filter. Integration time was set at 590 ms, and 3 images were captured every 0.45° through 180° rotation. Reconstruction was performed using SkyScan Recon software and analyzed using SkyScan CT Analysis software. Femoral trabecular parameters were measured on 250 slides (1.21 mm) of trabecular bone starting above the distal growth plate. Vertebral trabecular parameters were measured on 350 slides (1.72 mm) of trabecular bone between the two growth plates. Cortical femur parameters were measured on 75 slides (0.72 mm) at midshaft. For histological staining and dynamic histomorphometry, fixed femurs and tibiae were embedded in 4.5% methyl methacrylate. Five-micrometer-thick cross-sectional sections at the femoral midshaft and tibial longitudinal sections were collected using a Rotary microtome model RM2255 (Leica Microsystems). Sections were colored by Goldner staining; images were taken with a Leica DMR fluorescence microscope connected to a QImaging camera, and analysis used the BioquantOsteo software (BioQuant, Nashville, TN).

Blood biochemistry. Blood from 8-week-old male mice was taken at sacrifice by cardiac puncture. Serum was isolated using a serum separator tube (BD Microtainer tubes; BD, Franklin Lakes, NJ) following the manufacturer's instructions and stored at −80°C. The C-terminal telopeptide α1 chain of type I collagen (CTX) was detected using the RatLaps enzyme immunoassay (EIA) (Immunodiagnostic Systems, Scottsdale, AZ) following the manufacturer's instructions. Circulating carboxyglutamate (Gla)-osteocalcin and uncarboxylated glutamate (Glu)-osteocalcin were detected using enzyme-linked immunosorbent assay (ELISA) kits purchased from TaKaRa (catalog no. MK127 and MK129, respectively; Clontech Laboratories). Circulating fibroblast growth factor 23 (FGF23) levels were detected using an ELISA purchased from Kainos Laboratories (Tokyo, Japan). Quantification of calcium levels in serum was performed using Pointe Scientific calcium liquid reagents (catalog no. C7503-120; Thermo Fisher Scientific).

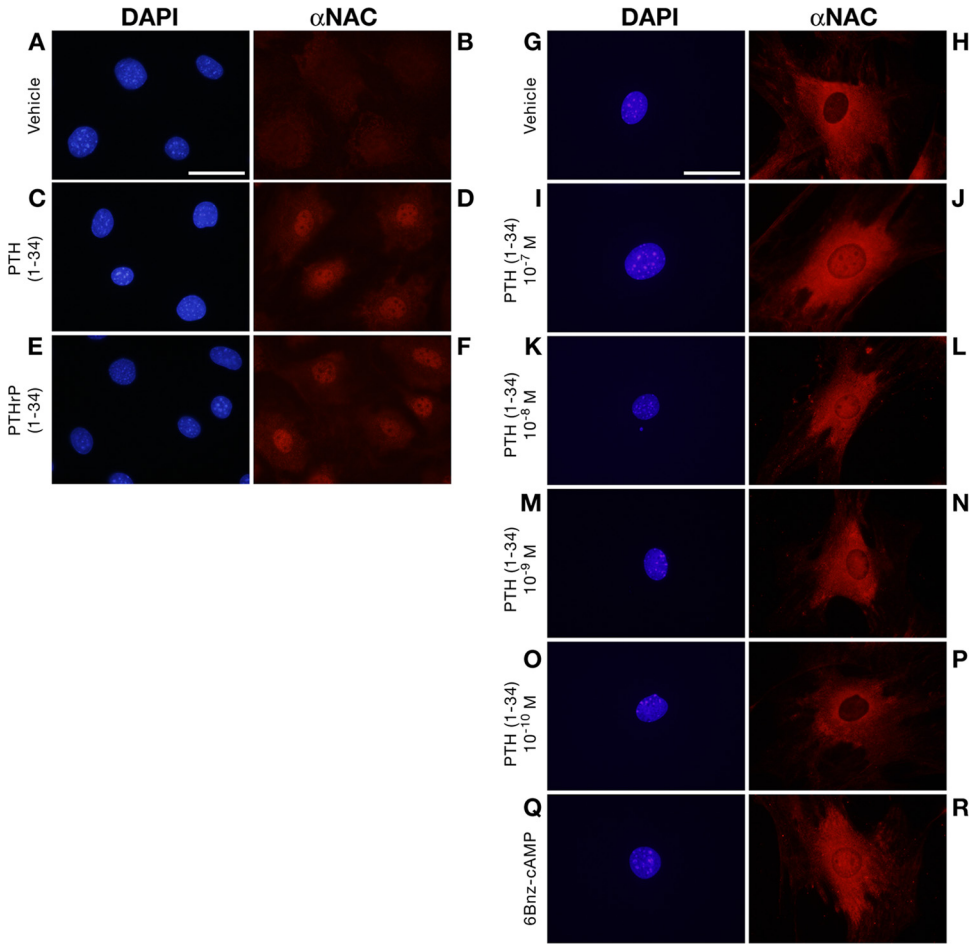

FIG 1 PTH and PTHrP induce nuclear translocation of αNAC. Shown are DAPI nuclear staining and immunofluorescence detection of endogenous αNAC in MC3T3-E1 cells (A to F) or primary cultures of osteoblasts (G to R). Cells were treated for 4 h with vehicle (A, B, G, and H), 10^{-7} M PTH(1–34) (C, D, I, and J), or increasing doses of PTH(1–34) ranging from 10^{-10} M to 10^{-8} M (K to P). MC3T3-E1 cultures were also treated with 10^{-7} M PTHrP(1–34) (E and F), while primary osteoblasts were exposed to the PKA-specific analog N^6-benzoyladenosine cAMP (6Bnz-cAMP) (Q and R). Images were obtained at 1,000×. Scale bar, 50 μm.

RT-qPCR. For reverse transcription-quantitative PCR (RT-qPCR), calvariae from 8-week-old male mice were collected in RNAlater (Life Technologies) and stored at −20°C until further processed. Calvariae were homogenized in 1 ml of TRIzol (Life technologies) using a Polytron PT-MR 300 (Kinematica AG, Littau, Switzerland), and RNA was extracted following the manufacturer's instructions. Using the high-capacity cDNA reverse transcription kit (Life Technologies), 1 μg of RNA was reverse transcribed into cDNA following the manufacturer's instructions. Gene expression monitoring was performed on 5% of the cDNA reaction mixture using TaqMan Universal PCR master mix (Life Technologies) with *Sost*, *RankL*, or *Opg* TaqMan assays. The β2-microglobulin gene (*B2m*) was used as the endogenous reference gene, and reactions were carried out in a 7500 real-time PCR system (Life Technologies Applied Biosystems). Data were analyzed using the SDS software from Applied Biosystems (Life technologies). Three or more samples per genotype were assayed in triplicate.

Statistical analysis. Statistical analysis was performed with analysis of variance with *post hoc* tests. A probability value (*P* value) lower than 0.05 was accepted as significant.

RESULTS

PTH-induced αNAC nuclear translocation is mediated by cAMP activation of PKA. Mice with a knock-in mutation preventing αNAC from translocating to the nucleus (17) show striking phenotype similarity to mice with osteoblast-specific inactivation of $G\alpha_s$ (13). This suggests that $G\alpha_s$ activation can lead to nuclear accumulation of αNAC. We looked at the effect of PTH, which activates $G\alpha_s$, on the subcellular localization of αNAC. The αNAC protein is detected in the cytosol of osteoblasts under steady-state conditions (Fig. 1A, B, G, and H and 2A and F). Upon treatment of MC3T3-E1 osteoblastic cells with 10^{-7} M PTH(1–34), the protein relocated to the nucleus (Fig. 1C and D). A similar nuclear translocation was observed when the cells were treated with PTHrP(1–34) (Fig. 1E and F), which also binds PTHR1 (32). PTH also dose dependently induced nuclear accumulation of αNAC in cultured primary osteoblasts. Nuclear translocation was readily observed in primary osteoblasts following treatment with 10^{-9} M PTH(1–34), and the effect was maintained over 2 orders of magnitude for doses (Fig. 1G to P).

To examine the signal transduction pathway involved, we used cell-permeable cAMP analogs and pathway inhibitors. The subcellular localization of αNAC was again assessed by immunofluorescence, and nuclei were identified by DAPI staining (Fig. 2A to E). We first stimulated MC3T3-E1 cells with dibutyryl-cAMP, a

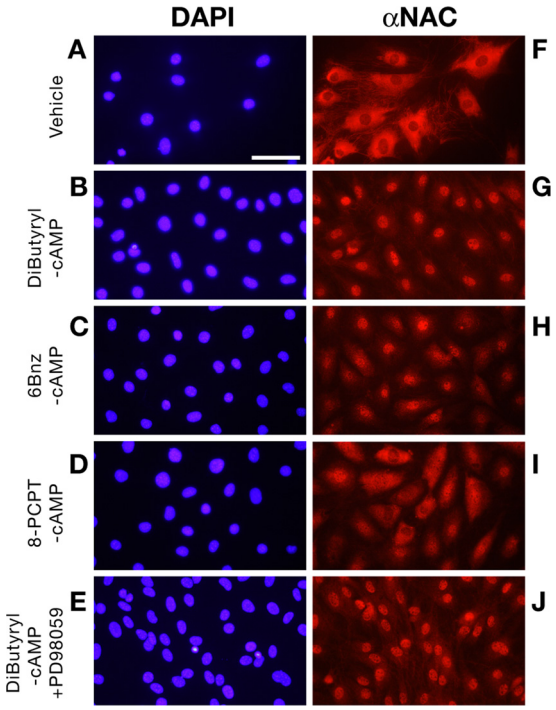

FIG 2 αNAC nuclear translocation involves cAMP-PKA signaling. Shown are DAPI nuclear staining (A to E) and immunofluorescence detection of endogenous αNAC (F to J) in MC3T3-E1 cells treated for 4 h with vehicle (A and F), dibutyryl-cAMP (B and G), the PKA-specific analog N^6-benzoyladenosine cAMP (6Bnz-cAMP) (C and H), the Epac-specific analog 8-(4-chlorophenylthio)-2′-*O*-methyladenosine cAMP (8-PCPT-cAMP) (D and I), or dibutyryl-cAMP with PD98059 (E and J). Magnification, ×400; scale bar, 100 μm.

non-pathway-specific analog. Treatment with dibutyryl-cAMP led to nuclear accumulation of αNAC (compare Fig. 2F and G), confirming that accumulation of cAMP triggers αNAC nuclear translocation. Stimulation with pathway-specific cAMP analogs further defined the mechanisms in play. αNAC relocated to the nucleus of cells treated with the PKA-specific analog N^6-benzoyladenosine cAMP (6Bnz-cAMP) (Fig. 1Q and R and 2C and H), while it remained cytosolic in cells exposed to the Epac pathway-specific analog 8-(4-chlorophenylthio)-2′-*O*-methyladenosine cAMP (8-PCPT-cAMP) (Fig. 2D and I). To further rule out the involvement of the Epac pathway, which involves several downstream effectors, including MEK1 (33), we treated cells with dibutyryl-cAMP (pathway nonspecific) and PD98059, a specific MEK1 inhibitor. The inhibitor did not prevent αNAC nuclear translocation (Fig. 2J). Taken together, these results suggest that PKA is the predominant effector kinase acting downstream from cAMP production to affect αNAC subcellular localization.

PKA phosphorylates αNAC at S99. *In silico* analysis of the αNAC protein sequence reveals a potential PKA phosphoacceptor site conserved across species, residue serine 99 (S99) (Fig. 3A). To ascertain that αNAC is a PKA substrate, we performed *in vitro* kinase assays with recombinant PKA and purified proteins (Fig. 3B). Bovine serum albumin (BSA) and cAMP response element binding protein (CREB) were used in the assay as negative and positive controls, respectively (lanes 1 and 2 and 7 and 8). Wild-type αNAC was phosphorylated by PKA (Fig. 3B, compare lanes 3 and 4). Replacement of serine 99 by an alanine residue (S99A) prevented PKA-mediated αNAC phosphorylation (lane 6).

We custom ordered an affinity-purified polyclonal antibody that recognizes the αNAC protein phosphorylated at amino acid S99 (anti-pS99) and validated its specificity using the *in vitro* kinase assay. Immunoblotting revealed that the anti-pS99 antibody exhibits high sensitivity and specificity. It dose dependently detected recombinant αNAC protein incubated with PKA (Fig. 3C, lanes 2 to 10), while it could not detect the highest concentration of αNAC not exposed to the kinase (lane 1). The previously described anti-αNAC antibody (24) recognized both unphosphorylated and phosphorylated forms of the protein indiscriminately (Fig. 3C, lower panel).

We used the anti-pS99 antibody to confirm that αNAC is phosphorylated in response to PTH treatment of osteoblastic cells. First, epitope-tagged wild-type or S99A-mutated αNAC proteins were expressed by retroviral infection in UMR-106 cells that were then stimulated with PTH(1–34) or the PKA-selective cAMP analog, 6Bnz-cAMP. Immunoprecipitation using anti-epitope tag antibodies followed by immunodetection with the αNAC antibody confirmed expression of the transfected proteins (Fig. 3D, bottom panel). Probing of the immunoprecipitates with the anti-pS99 antibody detected phosphorylated wild-type αNAC specifically in treated cells (Fig. 3D, top panel, compare lane 1 with lanes 2 and 3), but no signal was present in treated cells transfected with the S99A αNAC mutant (lanes 4 and 5). The anti-pS99 antibody also detected phosphorylated, endogenous wild-type αNAC in cultured primary osteoblasts treated with 100 μM 6Bnz-cAMP or PTH(1–34) from 10^{-9} to 10^{-7} M (Fig. 3E). To confirm that PKA is the kinase that phosphorylates αNAC downstream of PTH stimulation and cAMP accumulation in osteoblasts, we blocked endogenous PKA signaling by expressing a dominant-negative form of PKA (PKAdn) (26) in stably infected UMR-106 cells. Immunoblotting of whole-cell extracts was used to detect endogenous αNAC or transfected PKAdn, and even loading was monitored by probing for α-tubulin (Fig. 3F, bottom panel). The epitope-tagged PKAdn protein was detected in transfected cells but not in cells selected following transfection with an empty expression vector (Fig. 3F, third panel). All cell populations expressed endogenous αNAC (Fig. 3F, second panel). In vector-infected cells, stimulation with PTH(1–34) or 6Bnz-cAMP induced phosphorylation of αNAC at residue S99, as detected by probing with the anti-pS99 antibody (Fig. 3F, top panel, lanes 2 and 3). As shown on the immunoblot (Fig. 3F, top panel, lanes 4 to 6) and reflected by the quantification of the pS99/αNAC signal intensity ratio (Fig. 3F), the effects of PTH(1–34) and of the PKA-specific cAMP analog were dramatically decreased in cells expressing PKAdn. Taken together, these results show that αNAC is a substrate of PKA following PTH signaling.

Differential phosphorylation of αNAC at S99 regulates its subcellular localization. We compared the subcellular localization of wild-type and S99-mutated αNAC proteins following hormone or analog treatment to further understand the mechanisms implicated in PTH-induced αNAC nuclear translocation. Immunofluorescence detection of FLAG epitope-tagged αNAC proteins expressed in UMR-106 osteoblasts exposed to vehicle or treatment (Fig. 4A to I) was used to calculate the percentage of cells with nuclear αNAC localization (Fig. 4J). Wild-type αNAC was predominantly cytosolic (Fig. 4A), but treatment with PTH(1–34) (Fig. 4D) or 6Bnz-cAMP (Fig. 4G) induced significant nuclear translocation (Fig. 4J). Mutation of serine 99 to a nonphosphorylatable alanine residue (S99A) blocked PTH(1–34)- and 6Bnz-

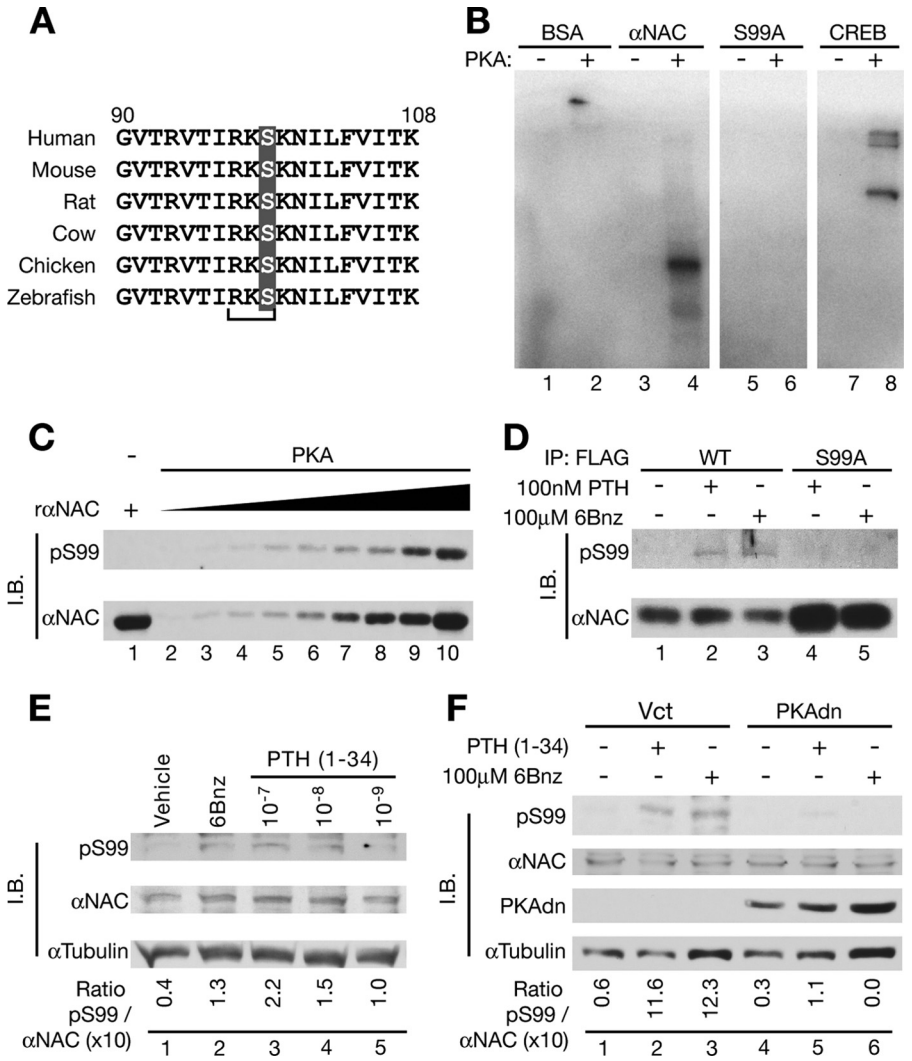

FIG 3 PKA phosphorylates αNAC on serine 99. (A) Cross-species alignment of the partial αNAC protein sequence between residues 90 to 108. The PKA recognition site is bracketed, and the phosphoacceptor residue serine 99 is highlighted. (B) Autoradiography of *in vitro* PKA phosphorylation assay performed using BSA (negative control) (lanes 1 and 2), wild-type αNAC (lanes 3 and 4), mutant S99 αNAC (S99A) (lanes 5 and 6), and recombinant CREB (positive control) (lanes 7 and 8) in the presence (+) or absence (−) of recombinant PKA. (C) Immunoblotting (I.B.) of *in vitro* PKA phosphorylation assay. Increasing amounts (lanes 2 to 10, 30, 44, 66, 100, 150, 222, 333, 500, and 1,000 ng, respectively; lane 1, 1,000 ng) of recombinant αNAC were incubated with (lanes 2 to 10) or without (lane 1) recombinant PKA. Transferred samples were probed with the phospho-specific anti-pS99 antibody (pS99) or anti-αNAC antibody. (D) UMR-106 cells were stably infected with FLAG epitope-tagged wild-type (WT) or mutant (S99A) αNAC and treated with PTH- or the PKA-specific cAMP analog N^6-benzoyladenosine cAMP (6Bnz-cAMP). Cell extracts were immunoprecipitated (I.P.) using anti-FLAG antibodies, and the immunoprecipitates were probed with the anti-pS99 antibody (pS99) or the anti-αNAC antibody. (E) Cultures of primary osteoblasts were treated with 100 μM 6Bnz-cAMP or the indicated doses (molar concentrations) of PTH(1–34). Total cell extracts were immunoblotted (I.B.) with either anti-pS99 antibody (pS99), anti-αNAC antibody, or anti-α-tubulin for a loading control. Quantification of the pS99/αNAC band signal intensity ratio is indicated below each track, above the track number. (F) UMR-106 cells were stably infected with an empty vector (Vct) or a myc-tagged-PKAdn expression vector and treated with vehicle (−), PTH(1–34) (100 nM), or 6Bnz-cAMP. Whole-cell extracts were separated by SDS-PAGE, transferred, and immunoblotted (I.B.) with anti-pS99, anti-αNAC, anti-myc epitope (PKAdn panel), or anti-α-tubulin for a loading control. Quantification of the pS99/αNAC band signal intensity ratio is indicated below each track, above the track number.

cAMP-induced αNAC nuclear translocation (Fig. 4B, E, H, and J). When serine 99 was replaced by a phosphomimetic aspartic acid residue (S99D), we observed statistically significant nuclear accumulation of αNAC, which was unaffected by treatment with the hormone or the cAMP analog (Fig. 4C, F, I, and J). These data strongly suggest that PTH treatment leads to differential phosphorylation of αNAC at S99 to regulate its subcellular localization.

PTH induces αNAC accumulation at the *Ocn* promoter through a PKA-dependent pathway. Nuclear αNAC binds to and regulates transcription from the *Ocn* promoter (16, 34). Since PTH induces αNAC nuclear translocation, we examined the effect of PTH or cAMP analog treatment on recruitment of wild-type or S99A αNAC proteins at the *Ocn* gene. Chromatin immunoprecipitation (ChIP) against endogenous αNAC following PTH(1–34) stimulation of MC3T3-E1 cells showed a significant 5-fold enrichment of the coregulator at its cognate binding site within the *Ocn* promoter compared to vehicle-treated cells (Fig. 5A). When the PKA-selective cAMP analog 6Bnz-cAMP was used to

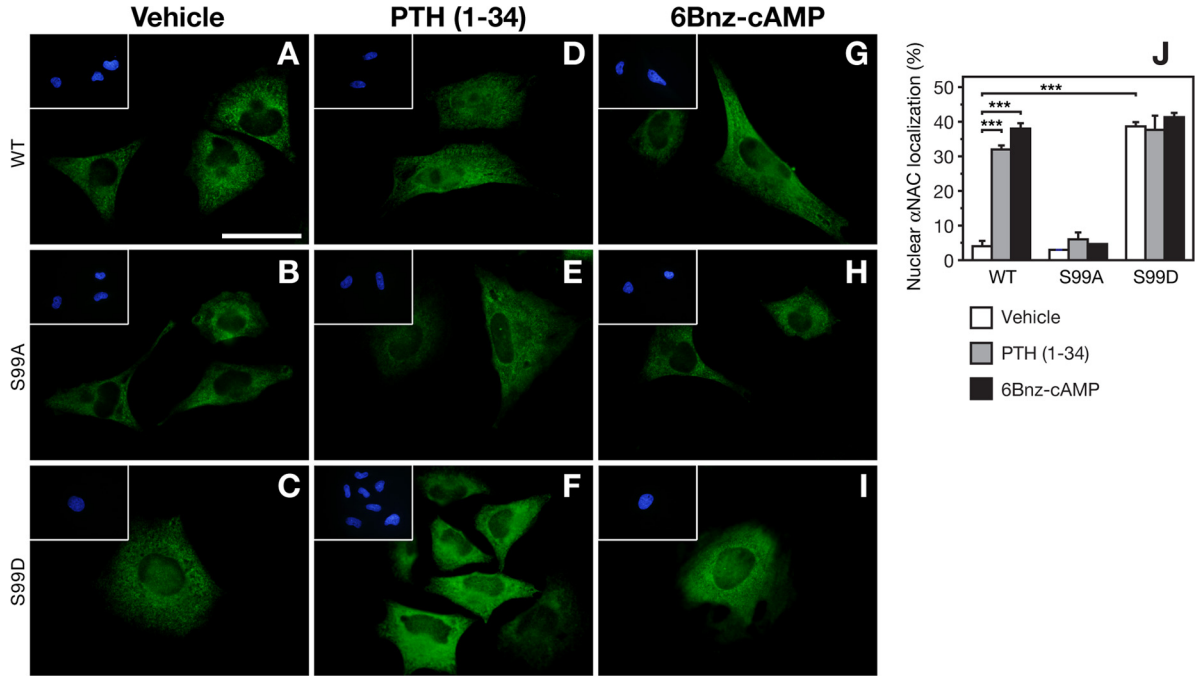

FIG 4 Serine 99 phosphorylation acts as a signal sending αNAC to the nucleus. UMR-106 cells were stably infected with FLAG epitope-tagged lentiviral expression vectors for the wild-type (WT) or S99A or S99D mutant αNAC and treated with vehicle (A to C), 10^{-7} M PTH(1–34) (D to F), or 100 μM 6Bnz-cAMP (G to I) for 4 h. (A to I) Representative results from immunodetection against the FLAG epitope are shown; DAPI staining is shown in the inset. Magnification, ×1,000; scale bar, 50 μm. (J) The graph depicts percentages established by counting the cells showing a positive nuclear signal after immunofluorescence against the FLAG epitope in 100 expressing cells from different microscopic fields. Data are presented as means ± SEM. ***, $P < 0.001$.

stimulate the osteoblasts we measured a significant 6.5-fold enrichment, supporting a PKA-dependent signal transduction pathway (Fig. 5A).

This conclusion is strengthened by results obtained in cells that stably express PKAdn. In control cells infected with the empty expression vector, PTH(1–34) or 6Bnz-cAMP treatment again caused significant enrichment of endogenous αNAC at the *Ocn* promoter (Fig. 5B, "Vector" bars). The PTH- or 6Bnz-cAMP-induced enrichment of αNAC at its target site was completely inhibited in cells expressing PKAdn (Fig. 5B, "PKAdn" bars), confirming that the PTH effect is PKA mediated.

To validate the implication of differential S99 phosphorylation in this mechanism, we next performed ChIP against the epitope tag in UMR-106 cells overexpressing FLAG-tagged wild-type or S99A αNAC. As previously observed with endogenous αNAC, PTH(1–34) or 6Bnz-cAMP treatment led to significant enrich-

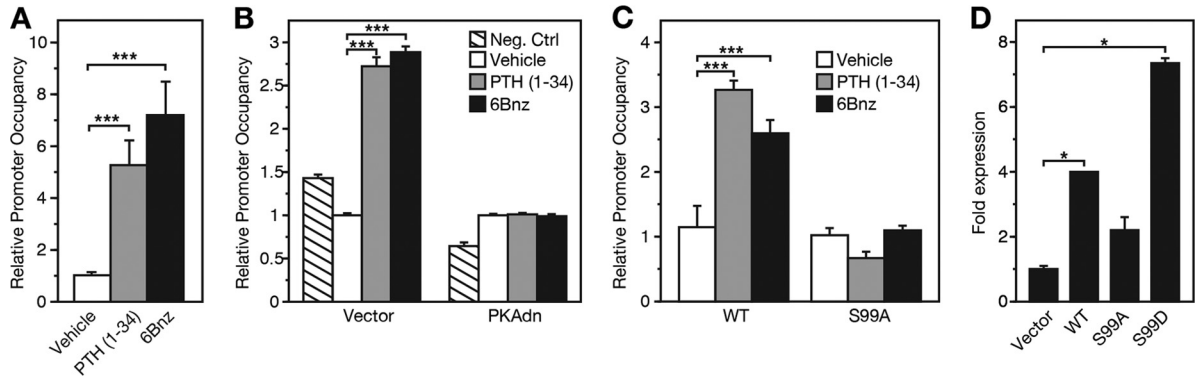

FIG 5 PTH-mediated αNAC accumulation at the *Ocn* promoter through a PKA-dependent pathway. (A to C) Quantitative chromatin immunoprecipitation (ChIP) assays in cells treated with vehicle, 100 nM PTH(1–34), or 100 μM 6Bnz-cAMP for 30 min. (A) MC3T3-E1 cells; (B) UMR-106 cells stably infected with an empty vector or a dominant-negative form of PKA (PKAdn); (C) UMR-106 cells stably expressing FLAG-tagged wild-type (WT) or S99A mutant αNAC. Quantitative ChIP assays were performed with anti-αNAC or anti-FLAG epitope antibody. ChIP products were amplified by SYBR green PCR using specific primers flanking the αNAC binding site in the *Ocn* promoter. Relative promoter occupancy was calculated as enrichment over vehicle-treated cells, which was ascribed an arbitrary value of 1. Results are means ± SEM of triplicate determinations. Neg. Ctrl, negative-control ChIP performed with naive IgG on cells treated for 30 min with 6Bnz-cAMP. (D) Reporter gene transient-transfection assay. UMR-106 cells were transfected with an *Ocn*-luc reporter plasmid and expression vectors for c-JUN in combination with wild-type αNAC or S99A or S99D mutant αNAC. Results are mean fold induction ± SEM, with luciferase levels measured in cells transfected with the empty expression vectors arbitrarily ascribed a value of 1. *, $P < 0.05$; ***, $P < 0.001$.

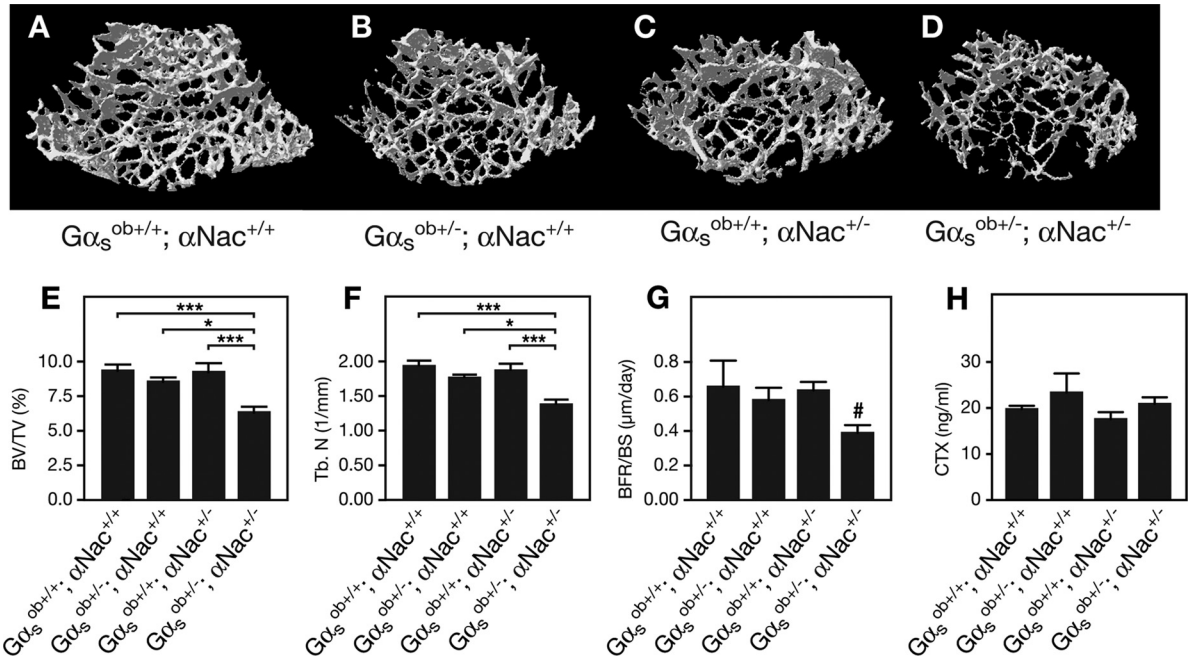

FIG 6 Osteopenia in compound $G\alpha_s^{ob+/-}$; $\alpha Nac^{+/-}$ heterozygous mice. (A to D) Three-dimensional reconstruction of 25-μm trabecular bone obtained by μCT from distal femur of control $G\alpha_s^{ob+/+}$; $\alpha Nac^{+/+}$, $G\alpha_s^{ob+/-}$; $\alpha Nac^{+/+}$, $G\alpha_s^{ob+/+}$; $\alpha Nac^{+/-}$ and compound $G\alpha_s^{ob+/-}$; $\alpha Nac^{+/-}$ mice. The scans were used to measure bone volume over tissue volume (BV/TV) (E) and trabecular number (Tb. N) (F) by analysis of 250 μm of trabecular bone under the primary spongiosa of the distal femur. (G) Mice were injected with calcein, and dynamic histomorphometry analysis was performed on femoral sections. Quantification confirmed significantly lower bone formation rates (BFR) when results from all control genotypes were grouped to increase statistical power. BS, bone surface (region segmented as bone). (H) Serum levels of C-terminal telopeptide (CTX). Graphed data are presented as means ± SEM from at least four mice per group. *, $P < 0.05$; ***, $P < 0.001$; #, $P < 0.05$ versus grouped genotype controls.

ment of epitope-tagged wild-type αNAC at the *Ocn* promoter (Fig. 5C). In contrast, mutation S99A completely abrogated the hormone- and analog-induced recruitment of αNAC at the target promoter (Fig. 5C).

Finally, we examined the effect of mutations at residue S99 on the transcriptional coactivation function of αNAC. UMR-106 cells were transfected with a reporter plasmid in which the luciferase gene is under the control of the *Ocn* proximal promoter (28) and expression vectors for c-JUN, alone or in combination with wild-type αNAC or S99A or S99D mutant αNAC. As previously reported (16), wild-type αNAC significantly potentiated c-JUN-mediated transcription from the *Ocn* promoter (Fig. 5D). This effect was abolished when residue S99 was mutated to an alanine but was enhanced by the phosphomimetic S99D mutation (Fig. 5D). We interpret the results shown in Fig. 5 to mean that PKA-mediated phosphorylation of αNAC at residue S99 leads to αNAC accumulation at the *Ocn* target promoter to enhance transcription.

Osteopenia and increased osteocyte numbers in $G\alpha_s$; αNAC compound heterozygotes. We altered gene dosage for $G\alpha_s$ and αNAC to find evidence that they form part of a common genetic pathway. To produce Osx1-GFP::Cre; $G\alpha_s^{+/fl}$; $\alpha NAC^{+/-}$ (abbreviated "$G\alpha_s^{ob+/-}$; $\alpha NAC^{+/-}$") compound heterozygous mice in which one allele of $G\alpha_s$ is specifically inactivated in *Osx*-expressing osteoblasts and one allele of αNAC is inactivated in all tissues, Osx-Cre; $\alpha Nac^{+/-}$ mice were crossed with $G\alpha_s^{fl/fl}$ mice. This allowed us to obtain all study genotypes in equivalent proportion: $G\alpha_s^{ob+/+}$; $\alpha Nac^{+/+}$, $G\alpha_s^{ob+/-}$; $\alpha Nac^{+/+}$, $G\alpha_s^{ob+/+}$; $\alpha Nac^{+/-}$, and $G\alpha_s^{ob+/-}$; $\alpha Nac^{+/-}$. There were no gross phenotypic manifestations for any of the genotypes studied (data not shown).

Mice heterozygous for either $G\alpha_s$ ($G\alpha_s^{ob+/-}$; $\alpha Nac^{+/+}$) or αNAC ($G\alpha_s^{ob+/+}$; $\alpha Nac^{+/-}$) alone exhibited no differences in femoral bone volume or trabecular number compared to wild-type ($G\alpha_s^{ob+/+}$; $\alpha Nac^{+/+}$) littermates (Fig. 6A, B, C, E, and F). The combined loss of one $G\alpha_s$ allele and one αNAC allele in bone cells caused a significant decrease in bone volume accompanied by a reduction in trabecular number in compound $G\alpha_s^{ob+/-}$; $\alpha Nac^{+/-}$ mice compared to all control genotypes (Fig. 6D to F). The compound gene dosage effect was restricted to trabecular parameters of the appendicular skeleton as we did not measure significant changes in cortical bone or in vertebrae (Table 1). Osteoblast activity was compared between genotypes using dynamic histomorphometry. Bone formation rates were unchanged and homogeneous between all control genotypes ($G\alpha_s^{ob+/+}$; $\alpha Nac^{+/+}$, $G\alpha_s^{ob+/-}$; $\alpha Nac^{+/+}$, and $G\alpha_s^{ob+/+}$; $\alpha Nac^{+/-}$) (Fig. 6G). When results from these animals were grouped to increase statistical power, we calculated a significant reduction in bone formation rates in compound $G\alpha_s^{ob+/-}$; $\alpha Nac^{+/-}$ mice (Fig. 6G). These results suggest that differences in osteoblast activity explain the reduced bone volume between compound heterozygotes and wild-type mice. This is further supported by the absence of impact of gene dosage alterations on serum parameters of bone resorption (type I collagen degradation products [CTX]) (Fig. 6H). Moreover, compound heterozygosity did not affect the *Rankl*/*Opg* mRNA ratio (1.08 ± 0.05, 1.06 ± 0.03, 1.00 ± 0.02, and 0.97 ± 0.02 for $G\alpha_s^{ob+/+}$; $\alpha Nac^{+/+}$, $G\alpha_s^{ob+/-}$; $\alpha Nac^{+/+}$, $G\alpha_s^{ob+/+}$; $\alpha Nac^{+/-}$, and $G\alpha_s^{ob+/-}$; $\alpha Nac^{+/-}$ mice, respectively; $P = 0.108$).

Blood analysis revealed no difference in the levels of steady-state calcium or FGF23 (Table 2). Relative levels of circulating carboxyglutamate (Gla)-osteocalcin and uncarboxylated gluta-

TABLE 1 Cortical and vertebral bone parameters[a]

Mouse phenotype	Cortical bone					Vertebrae	
	Cortical bone area/total area (%)	Avg cortical thickness (mm)	Periosteal perimeter (mm)	Endocortical perimeter (mm)	Total area (mm^2)	BV/TV ratio (%)	Trabecular no. (1/mm)
$G\alpha_s^{ob+/+}$; $\alpha NAC^{+/+}$	38.54 ± 0.93	0.156 ± 0.006	5.37 ± 0.15	4.22 ± 0.13	1.95 ± 0.11	16.11 ± 0.55	4.10 ± 0.12
$G\alpha_s^{ob+/-}$; $\alpha NAC^{+/+}$	34.27 ± 0.82	0.132 ± 0.006	5.07 ± 0.17	4.12 ± 0.17	1.77 ± 0.13	13.85 ± 1.21	3.69 ± 0.17
$G\alpha_s^{ob+/+}$; $\alpha NAC^{+/-}$	38.62 ± 1.08	0.155 ± 0.006	5.27 ± 0.11	4.14 ± 0.08	1.89 ± 0.08	15.50 ± 0.75	3.83 ± 0.08
$G\alpha_s^{ob+/-}$; $\alpha NAC^{+/-}$	35.03 ± 0.61	0.127 ± 0.003	4.76 ± 0.11	3.81 ± 0.10	1.56 ± 0.07	14.93 ± 0.46	3.73 ± 0.10

[a] The parameters shown are based on the definition and description guidelines from reference 57. Cortical bone area = cortical vol/(no. of slices × slice thickness). Total area represents the total cross-sectional area inside the periosteal envelope. The BV/TV ratio (i.e., bone volume fraction) represents the ratio of the segmented bone volume to the total volume of the region of interest. The trabecular number represents the average number of trabeculae per unit length.

mate (Glu)-osteocalcin were also unchanged in compound heterozygotes compared to wild-type littermates (Table 2). Taken together, the blood biochemistry results show that changes in $G\alpha_s$ and αNAC gene dosage do not cause endocrine dysfunction.

One shared phenotypic manifestation between $\alpha NAC^{S43A/S43A}$ and Osx-CRE; $G\alpha_s^{fl/fl}$ mutant mice is an increased number of osteocytes measured in cortical bone (13, 17). We thus counted the osteocytes present in cortical bone at the femoral midshaft following alteration in gene dosage for $G\alpha_s$ and αNAC (Fig. 7A to D). We measured a significant increase in the number of osteocytes per mm^2 in compound $G\alpha_s^{ob+/-}$; $\alpha Nac^{+/-}$ heterozygous mice compared to all control genotypes (Fig. 7E). This was accompanied by significantly augmented expression of the osteocyte marker gene *Sost* (Fig. 7F). These results confirm the genetic link between $G\alpha_s$ and αNAC.

DISCUSSION

We have previously shown using knock-in gene targeting that mutation of the integrin-linked kinase phosphoacceptor site within αNAC (residue serine 43) affects its nuclear translocation and impacts bone development (17). The S43A mutation only partially decreased αNAC nuclear accumulation (17), suggesting that other pathways and mechanisms could direct the transcriptional coregulator to the nucleus. Based on the phenotypic similarities between the $\alpha NAC^{S43A/S43A}$ knock-in mice and mice with osteoblast-specific inactivation of $G\alpha_s$ (13, 17), we hypothesized that αNAC could act as an effector downstream of $G\alpha_s$ activation. Here we present results that support a PTH-$G\alpha_s$-PKA-αNAC signal transduction pathway leading to phosphorylation-mediated nuclear translocation of αNAC to regulate target gene expression. The physiological relevance of this pathway is supported by the phenotypic manifestation observed in compound $G\alpha_s^{ob+/-}$; $\alpha NAC^{+/-}$ heterozygotes, which suggests that nuclear αNAC could be involved in mediating the anabolic action of PTH on bone.

PKA is known to phosphorylate proteins containing a dibasic motif, R-R/K-X-S/T (35–37). More rarely, the kinase was shown to phosphorylate nonclassical monobasic motifs, such as R-X-X-S/T and R-X-S/T, which are weaker phosphoacceptor sites (37). The αNAC protein sequence does not harbor a classical dibasic motif, but several observations confirm that the atypical -R-K-S- site within the αNAC sequence is functional. Mutation of residue serine 99 blocked PKA-mediated αNAC phosphorylation, PTH-induced αNAC nuclear translocation, and recruitment to the *Ocn* promoter. Expression of a dominant-negative PKA moiety prevented phosphorylation at S99 and *Ocn* promoter occupancy following PTH- or PKA-specific cAMP analog treatment. It appears that phosphorylation at S99 results in rapid shuttling of αNAC to the nucleus since we detected increased recruitment of αNAC at the *Ocn* promoter within 30 min following PTH stimulation of osteoblasts. Our results suggest that S99 phosphorylation not only serves as a signal to send αNAC to the nucleus but also acts as a switch to activate it, at least at the *Ocn* target promoter. Expression of a phosphomimetic mutant of αNAC (S99D) mimicked the effect of PTH on both αNAC nuclear localization and regulation of *Ocn* gene expression.

As previously mentioned, parallel mechanisms, such as phosphorylation by integrin-linked kinase, exist to regulate the subcellular localization of αNAC (17, 19). While both signals may work cooperatively to maximize αNAC nuclear entry, it is also possible that cells have developed separate pathways for αNAC nuclear translocation in response to hormonal stimulus or integrin-mediated adhesion cues. Further experiments will be required to elucidate this point.

The molecular and cellular mechanisms responsible for the bone-forming effect of intermittent PTH treatment are not fully understood. Among the characterized responses to PTH, the cAMP response element binding protein, CREB, was shown to be phosphorylated (38). CREB then stimulates the transcription of members of genes coding for the AP-1 family of basic domain-

TABLE 2 Blood biochemistry results

Mouse phenotype	Concn in blood of[a]:			
	Gla-OCN (ng/ml)	Glu-OCN (ng/ml)	FGF23 (pg/ml)	Calcium (mmol/liter)
$G\alpha_s^{ob+/+}$; $\alpha NAC^{+/+}$	235.1 ± 27.1	4.33 ± 0.27	89.39 ± 15.08	2.27 ± 0.04
$G\alpha_s^{ob+/-}$; $\alpha NAC^{+/+}$	149.9 ± 21.5	4.37 ± 0.50	111.10 ± 12.50	2.40 ± 0.14
$G\alpha_s^{ob+/+}$; $\alpha NAC^{+/-}$	144.1 ± 18.2	4.12 ± 0.51	81.18 ± 3.62	2.11 ± 0.16
$G\alpha_s^{ob+/-}$; $\alpha NAC^{+/-}$	142.2 ± 30.6	4.16 ± 0.42	100.90 ± 9.34	2.30 ± 0.16

[a] Gla-OCN, carboxyglutamate-osteocalcin; Glu-OCN, uncarboxylated glutamate-osteocalcin.

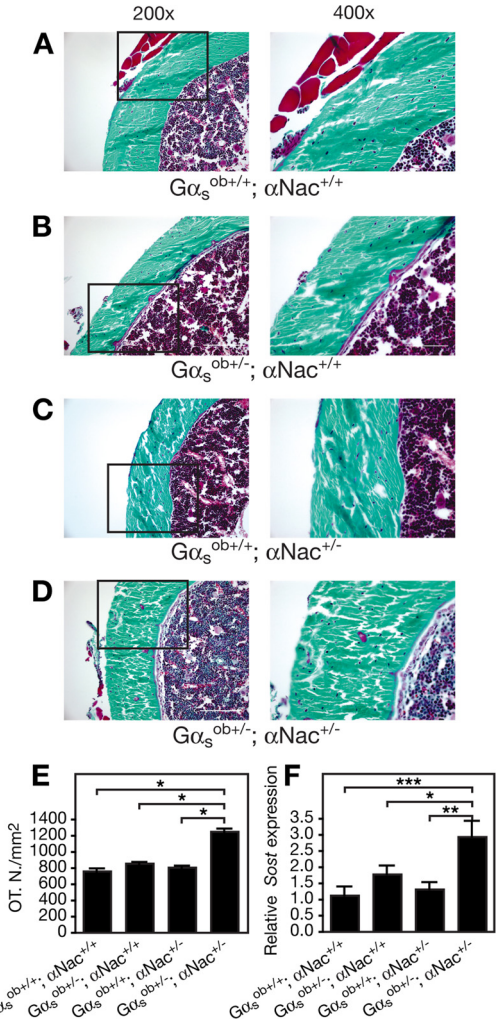

FIG 7 Increased numbers of osteocytes in compound $G\alpha_s^{ob+/-}$; $\alpha Nac^{+/-}$ heterozygous mice. (A to D) Goldner's staining of femoral cross sections at midshaft from control $G\alpha_s^{ob+/+}$; $\alpha Nac^{+/+}$, $G\alpha_s^{ob+/-}$; $\alpha Nac^{+/+}$, $G\alpha_s^{ob+/+}$; $\alpha Nac^{+/-}$ and compound $G\alpha_s^{ob+/-}$; $\alpha Nac^{+/-}$ mice. Right, higher-magnification (400) views of the boxed area on the left (200). (E) Osteocyte number (OT.N.) per surface area in femoral cortex. Data are presented as means ± SEM from at least three mice per group. (F) Quantitative reverse-transcription PCR of *Sost* gene expression using mRNA isolated from mouse calvaria at 8 weeks of age. The *B2m* gene was used as a housekeeping reference. Data are expressed relative to levels measured in wild-type ($G\alpha_s^{ob+/+}$; $\alpha Nac^{+/+}$) littermates and presented as the means ± SEM of at least three mice per group. *, $P < 0.05$; **, $P < 0.01$; ***, $P < 0.001$.

leucine zipper transcription factors, c-*Fos* and c-*Jun* (38–40). While the importance of AP-1 proteins in mediating the anabolic PTH response remains to be determined, it is noteworthy that αNAC interacts with the N-terminal activation domain of c-JUN to regulate transcription (16, 20, 21, 41). Interaction with c-JUN involves residues 89 to 129 within αNAC (41), a region containing 5 β-sheets (42). Residue S99 is located at the extremity of the second β-sheet structure that plays a physical role for αNAC heterodimerization with βNAC (42). It is tempting to speculate that phosphorylation of serine 99 displaces βNAC and allows nuclear translocation of the α subunit. PTH stimulation led to αNac enrichment at the *Ocn* promoter, and a phosphomimetic residue substitution at position 99 enhanced the coactivation potential of αNAC. It is thus possible that phosphorylated S99 helps to stabilize the complex formed by αNAC and c-JUN on specific target gene promoters.

A mechanism associated with the deletion of $G\alpha_s$ in early osteoblasts involved diminished WNT signaling caused by increased expression of the inhibitors of the WNT pathway, *Sost* and *Dickkopf1* (13). The expression of the osteocyte differentiation marker *Sost* was also elevated in compound $G\alpha_s^{ob+/-}$; $\alpha NAC^{+/-}$ heterozygotes. Osteocytes, the most abundant cell type in bone, result from osteoblast maturation. Like osteoblasts, they express PTH1R and can answer to PTH stimulation through a PKA-dependent pathway (43–45). One of the main effects of PTH on osteocytes is the suppression of *Sost* expression through an MEF2-dependent mechanism (46). It has also been shown that osteocyte-specific deletion of PTH1R leads to a reduction in trabecular bone mass (47, 48). As previously mentioned, osteopenia, increased number of osteocytes, and increased expression of *Sost* are common features observed in $\alpha Nac^{S43A/S43A}$, Osx-CRE; $G\alpha_s^{fl/fl}$, and $G\alpha_s^{ob+/-}$; $\alpha Nac^{+/-}$ mice. This supports the notion that nuclear αNAC is important to regulate osteoblast maturation into osteocytes but also raises the possibility that αNAC is involved in PTH signaling in osteocytes. The compound mouse model that we generated does not allow discrimination between the function of αNAC in osteoblasts or osteocytes since the αNAC disruption is systemic and the $G\alpha_{s^{fl/fl}}$ allele recombination was under the control of the CRE recombinase coupled to the *Osx* promoter, expressed in both osteoblasts and osteocytes (30). Nevertheless, the hypothesis of a potential role for αNAC in osteocytes is supported by our preliminary observation that stimulation of the MLOY4 osteocyte cell line (49) with PTH(1–34) induces αNAC nuclear translocation (M. Pellicelli and R. St-Arnaud, unpublished observation).

More recently, increased trabecular bone mass and reduced *Sost* expression were reported in mice specifically expressing a constitutively active form of PKA (CA-PKA) in late osteoblasts and in osteocytes (50). A similar phenotype has been observed in transgenic mice expressing a constitutively active form of PTH1R (CA-PTH1R) in osteocytes (51, 52). However, there exists some discrepancy between the reported phenotypes. In addition to the increase in bone trabecular volume and reduced *Sost* expression, CA-PTH1R mice presented an increased cortical thickness and an increase in bone turnover (51, 52). These differences support the idea that PTH effects are mediated using other pathways in addition to PKA-dependent signaling. We did not detect changes in cortical bone thickness in compound $G\alpha_s^{ob+/-}$; $\alpha Nac^{+/-}$ heterozygous mice, and their bone mass phenotype was limited to trabecular bone. This observation supports the notion that αNAC is part of a PKA-dependent pathway in osteocytes to regulate trabecular bone volume.

Compound $G\alpha_s^{ob+/-}$; $\alpha Nac^{+/-}$ heterozygotes also sported increased numbers of cortical osteocytes, with associated elevated *Sost* expression. The *Sost* increase could be the result of the augmented osteocyte number in the mutant mice. However, the increase in osteocyte density appears too modest to explain the change in mRNA levels. Our preferred interpretation is that αNAC is an effector of PKA signaling in osteocytes to suppress *Sost* expression. We have shown that αNAC differentially interacts with transcriptional corepressors to control gene expression in cell- and promoter-specific contexts (34), and our most recent results indicate that this interaction is phosphorylation dependent (53). This suggests an appealing mechanism through which PKA-

modified, phospho-S99-αNAC would recruit transcriptional corepressors to inhibit *Sost* transcription in osteocytes. The cell- and promoter-specific context of this model is highlighted by the increased transcription from the *Ocn* promoter that we measured in transient-transfection assays using the S99D phosphomimetic mutant in osteoblasts (Fig. 5D). We will test the physiological relevance of this proposed mechanism using site-directed mutagenesis of αNAC at S99 in knock-in mouse models.

Ocn remains the best-characterized transcriptional target of αNAC to date (16), although *in vitro* studies and mutant mouse models have hinted at other relevant promoters (17, 34, 54). The regulatory pathway characterized in this study broadens the set of putative targets regulated by αNAC. Genes that are regulated by both PTH and c-JUN, the transcriptional partner of αNAC, are appealing potential candidates. These include *Mmp13* and c-*Jun* itself (39, 55, 56) in addition to *Ocn*. Additional experiments using ChIP-Seq analysis of PTH-treated osteoblasts or osteocytes, or cells expressing epitope-tagged S99D αNAC, have been initiated to further our knowledge of αNAC-dependent transcriptional control.

The anabolic activity of PTH on bone is a complex response involving many pathways. However, many studies have confirmed the major contribution of the $G\alpha_s$-cAMP-PKA signaling cascade in this response. Our results identifying αNAC as a new direct effector of PTH-$G\alpha_s$-cAMP-PKA signaling affecting bone mass suggest that αNAC is needed for the anabolic action of PTH on bone.

ACKNOWLEDGMENTS

We thank N. O. Dulin (University of Chicago) for providing the PKAdn expression vector and A. P. McMahon (Harvard University) and L. S. Weinstein (NIH) for access to the Osx1-GFP::Cre and $G\alpha_s^{fl/fl}$ mouse strains, respectively. Guylaine Bédard and Mark Lepik prepared the figures. We used the microcomputed tomography instrument of the McGill University Health Center Orthopaedic Research division and acknowledge support from the Network for Oral and Bone Health Research for aiding access to this infrastructure.

M.P. holds a Shriners Hospitals for Children Postdoctoral Fellowship award. This work was supported by NIH grant AR54741 to J.Y.W. and by an operating grant from the Canadian Institutes for Health Research (MOP-119306) to R.S.-A.

REFERENCES

1. **Levine MA.** 2003. Normal mineral homeostasis. Interplay of parathyroid hormone and vitamin D. Endocr. Dev. **6:**14–33. http://dx.doi.org/10.1159/000072764.
2. **Dobnig H, Turner RT.** 1997. The effects of programmed administration of human parathyroid hormone fragment (1–34) on bone histomorphometry and serum chemistry in rats. Endocrinology **138:**4607–4612. http://dx.doi.org/10.1210/endo.138.11.5505.
3. **Frolik CA, Black EC, Cain RL, Satterwhite JH, Brown-Augsburger PL, Sato M, Hock JM.** 2003. Anabolic and catabolic bone effects of human parathyroid hormone (1–34) are predicted by duration of hormone exposure. Bone **33:**372–379. http://dx.doi.org/10.1016/S8756-3282(03)00202-3.
4. **Iida-Klein A, Zhou H, Lu SS, Levine LR, Ducayen-Knowles M, Dempster DW, Nieves J, Lindsay R.** 2002. Anabolic action of parathyroid hormone is skeletal site specific at the tissue and cellular levels in mice. J. Bone Miner. Res. **17:**808–816. http://dx.doi.org/10.1359/jbmr.2002.17.5.808.
5. **Jilka RL.** 2007. Molecular and cellular mechanisms of the anabolic effect of intermittent PTH. Bone **40:**1434–1446. http://dx.doi.org/10.1016/j.bone.2007.03.017.
6. **Lanske B, Kronenberg HM.** 1998. Parathyroid hormone-related peptide (PTHrP) and parathyroid hormone (PTH)/PTHrP receptor. Crit. Rev. Eukaryot. Gene Expr. **8:**297–320. http://dx.doi.org/10.1615/CritRevEukarGeneExpr.v8.i3-4.40.
7. **Datta NS, Abou-Samra AB.** 2009. PTH and PTHrP signaling in osteoblasts. Cell Signal. **21:**1245–1254. http://dx.doi.org/10.1016/j.cellsig.2009.02.012.
8. **Gloerich M, Bos JL.** 2010. Epac: defining a new mechanism for cAMP action. Annu. Rev. Pharmacol. Toxicol. **50:**355–375. http://dx.doi.org/10.1146/annurev.pharmtox.010909.105714.
9. **Fujita T, Meguro T, Fukuyama R, Nakamuta H, Koida M.** 2002. New signaling pathway for parathyroid hormone and cyclic AMP action on extracellular-regulated kinase and cell proliferation in bone cells. Checkpoint of modulation by cyclic AMP. J. Biol. Chem. **277:**22191–22200. http://dx.doi.org/10.1074/jbc.M110364200.
10. **Iida-Klein A, Guo J, Drake MT, Kronenberg HM, Abou-Samra AB, Bringhurst FR, Segre GV.** 1995. Structural requirements of parathyroid hormone/parathyroid hormone-related peptide receptors for phospholipase C activation and regulation of phosphate uptake. Miner. Electrolyte Metab. **21:**177–179.
11. **Armamento-Villareal R, Ziambaras K, Abbasi-Jarhomi SH, Dimarogonas A, Halstead L, Fausto A, Avioli LV, Civitelli R.** 1997. An intact N terminus is required for the anabolic action of parathyroid hormone on adult female rats. J. Bone Miner. Res. **12:**384–392. http://dx.doi.org/10.1359/jbmr.1997.12.3.384.
12. **Takasu H, Gardella TJ, Luck MD, Potts JT, Jr, Bringhurst FR.** 1999. Amino-terminal modifications of human parathyroid hormone (PTH) selectively alter phospholipase C signaling via the type 1 PTH receptor: implications for design of signal-specific PTH ligands. Biochemistry **38:**13453–13460. http://dx.doi.org/10.1021/bi990437n.
13. **Wu JY, Aarnisalo P, Bastepe M, Sinha P, Fulzele K, Selig MK, Chen M, Poulton IJ, Purton LE, Sims NA, Weinstein LS, Kronenberg HM.** 2011. Gsalpha enhances commitment of mesenchymal progenitors to the osteoblast lineage but restrains osteoblast differentiation in mice. J. Clin. Invest. **121:**3492–3504. http://dx.doi.org/10.1172/JCI46406.
14. **Hernandez CJ, Majeska RJ, Schaffler MB.** 2004. Osteocyte density in woven bone. Bone **35:**1095–1099. http://dx.doi.org/10.1016/j.bone.2004.07.002.
15. **Noble BS, Reeve J.** 2000. Osteocyte function, osteocyte death and bone fracture resistance. Mol. Cell Endocrinol. **159:**7–13. http://dx.doi.org/10.1016/S0303-7207(99)00174-4.
16. **Akhouayri O, Quelo I, St-Arnaud R.** 2005. Sequence-specific DNA binding by the alphaNAC coactivator is required for potentiation of c-Jun-dependent transcription of the osteocalcin gene. Mol. Cell. Biol. **25:**3452–3460. http://dx.doi.org/10.1128/MCB.25.9.3452-3460.2005.
17. **Meury T, Akhouayri O, Jafarov T, Mandic V, St-Arnaud R.** 2010. Nuclear alpha NAC influences bone matrix mineralization and osteoblast maturation in vivo. Mol. Cell. Biol. **30:**43–53. http://dx.doi.org/10.1128/MCB.00378-09.
18. **McDonald PC, Fielding AB, Dedhar S.** 2008. Integrin-linked kinase—essential roles in physiology and cancer biology. J. Cell Sci. **121:**3121–3132. http://dx.doi.org/10.1242/jcs.017996.
19. **Quelo I, Gauthier C, Hannigan GE, Dedhar S, St-Arnaud R.** 2004. Integrin-linked kinase regulates the nuclear entry of the c-Jun coactivator alpha-NAC and its coactivation potency. J. Biol. Chem. **279:**43893–43899. http://dx.doi.org/10.1074/jbc.M406310200.
20. **Akhouayri O, St-Arnaud R.** 2007. Differential mechanisms of transcriptional regulation of the mouse osteocalcin gene by jun family members. Calcif. Tissue Int. **80:**123–131. http://dx.doi.org/10.1007/s00223-006-0102-7.
21. **Moreau A, Yotov WV, Glorieux FH, St-Arnaud R.** 1998. Bone-specific expression of the alpha chain of the nascent polypeptide-associated complex, a coactivator potentiating c-Jun-mediated transcription. Mol. Cell. Biol. **18:**1312–1321.
22. **Sudo H, Kodama HA, Amagai Y, Yamamoto S, Kasai S.** 1983. In vitro differentiation and calcification in a new clonal osteogenic cell line derived from newborn mouse calvaria. J. Cell Biol. **96:**191–198. http://dx.doi.org/10.1083/jcb.96.1.191.
23. **Bringhurst FR, Zajac JD, Daggett AS, Skurat RN, Kronenberg HM.** 1989. Inhibition of parathyroid hormone responsiveness in clonal osteoblastic cells expressing a mutant form of 3′,5′-cyclic adenosine monophosphate-dependent protein kinase. Mol. Endocrinol. **3:**60–67. http://dx.doi.org/10.1210/mend-3-1-60.
24. **Yotov WV, St-Arnaud R.** 1996. Differential splicing-in of a proline-rich

exon converts alphaNAC into a muscle-specific transcription factor. Genes Dev. **10:**1763–1772. http://dx.doi.org/10.1101/gad.10.14.1763.
25. **Bakker AD, Klein-Nulend J.** 2012. Osteoblast isolation from murine calvaria and long bones. Methods Mol. Biol. **816:**19–29. http://dx.doi.org/10.1007/978-1-61779-415-5_2.
26. **Andreassen TT, Ejersted C, Oxlund H.** 1999. Intermittent parathyroid hormone (1–34) treatment increases callus formation and mechanical strength of healing rat fractures. J. Bone Miner. Res. **14:**960–968. http://dx.doi.org/10.1359/jbmr.1999.14.6.960.
27. **Wazen RM, Moffatt P, Zalzal SF, Daniel NG, Westerman KA, Nanci A.** 2006. Local gene transfer to calcified tissue cells using prolonged infusion of a lentiviral vector. Gene Ther. **13:**1595–1602. http://dx.doi.org/10.1038/sj.gt.3302824.
28. **Ducy P, Karsenty G.** 1995. Two distinct osteoblast-specific cis-acting elements control expression of a mouse osteocalcin gene. Mol. Cell. Biol. **15:**1858–1869.
29. **Chen M, Gavrilova O, Zhao WQ, Nguyen A, Lorenzo J, Shen L, Nackers L, Pack S, Jou W, Weinstein LS.** 2005. Increased glucose tolerance and reduced adiposity in the absence of fasting hypoglycemia in mice with liver-specific Gs alpha deficiency. J. Clin. Invest. **115:**3217–3227. http://dx.doi.org/10.1172/JCI24196.
30. **Rodda SJ, McMahon AP.** 2006. Distinct roles for Hedgehog and canonical Wnt signaling in specification, differentiation and maintenance of osteoblast progenitors. Development **133:**3231–3244. http://dx.doi.org/10.1242/dev.02480.
31. **Hekmatnejad B, Mandic V, Yu VW, Akhouayri O, Arabian A, St-Arnaud R.** 2014. Altered gene dosage confirms the genetic interaction between FIAT and alphaNAC. Gene http://dx.doi.org/10.1016/j.gene.2014.01.009.
32. **Mannstadt M, Juppner H, Gardella TJ.** 1999. Receptors for PTH and PTHrP: their biological importance and functional properties. Am. J. Physiol. **277:**F665–F675.
33. **Laroche-Joubert N, Marsy S, Michelet S, Imbert-Teboul M, Doucet A.** 2002. Protein kinase A-independent activation of ERK and H,K-ATPase by cAMP in native kidney cells: role of Epac I. J. Biol. Chem. **277:**18598–18604. http://dx.doi.org/10.1074/jbc.M201868200.
34. **Jafarov T, Alexander JW, St-Arnaud R.** 2012. alphaNAC interacts with histone deacetylase corepressors to control myogenin and osteocalcin gene expression. Biochim. Biophys. Acta **1819:**1208–1216. http://dx.doi.org/10.1016/j.bbagrm.2012.10.005.
35. **Zetterqvist O, Ragnarsson U, Humble E, Berglund L, Engstrom L.** 1976. The minimum substrate of cyclic AMP-stimulated protein kinase, as studied by synthetic peptides representing the phosphorylatable site of pyruvate kinase (type L) of rat liver. Biochem. Biophys. Res. Commun. **70:**696–703. http://dx.doi.org/10.1016/0006-291X(76)90648-3.
36. **Kemp BE, Graves DJ, Benjamini E, Krebs EG.** 1977. Role of multiple basic residues in determining the substrate specificity of cyclic AMP-dependent protein kinase. J. Biol. Chem. **252:**4888–4894.
37. **Kennelly PJ, Krebs EG.** 1991. Consensus sequences as substrate specificity determinants for protein kinases and protein phosphatases. J. Biol. Chem. **266:**15555–15558.
38. **Pearman AT, Chou WY, Bergman KD, Pulumati MR, Partridge NC.** 1996. Parathyroid hormone induces c-fos promoter activity in osteoblastic cells through phosphorylated cAMP response element (CRE)-binding protein binding to the major CRE. J. Biol. Chem. **271:**25715–25721. http://dx.doi.org/10.1074/jbc.271.41.25715.
39. **Clohisy JC, Scott DK, Brakenhoff KD, Quinn CO, Partridge NC.** 1992. Parathyroid hormone induces c-fos and c-jun messenger RNA in rat osteoblastic cells. Mol. Endocrinol. **6:**1834–1842. http://dx.doi.org/10.1210/mend.6.11.1480173.
40. **McCauley LK, Koh AJ, Beecher CA, Rosol TJ.** 1997. Proto-oncogene c-fos is transcriptionally regulated by parathyroid hormone (PTH) and PTH-related protein in a cyclic adenosine monophosphate-dependent manner in osteoblastic cells. Endocrinology **138:**5427–5433. http://dx.doi.org/10.1210/endo.138.12.5587.
41. **Quelo I, Hurtubise M, St-Arnaud R.** 2002. alphaNAC requires an interaction with c-Jun to exert its transcriptional coactivation. Gene Expr. **10:**255–262.
42. **Liu Y, Hu Y, Li X, Niu L, Teng M.** 2010. The crystal structure of the human nascent polypeptide-associated complex domain reveals a nucleic acid-binding region on the NACA subunit. Biochemistry **49:**2890–2896. http://dx.doi.org/10.1021/bi902050p.
43. **Fermor B, Skerry TM.** 1995. PTH/PTHrP receptor expression on osteoblasts and osteocytes but not resorbing bone surfaces in growing rats. J. Bone Miner. Res. **10:**1935–1943.
44. **Bodine PV, Vernon SK, Komm BS.** 1996. Establishment and hormonal regulation of a conditionally transformed preosteocytic cell line from adult human bone. Endocrinology **137:**4592–4604. http://dx.doi.org/10.1210/endo.137.11.8895322.
45. **van der Plas A, Aarden EM, Feijen JH, de Boer AH, Wiltink A, Alblas MJ, de Leij L, Nijweide PJ.** 1994. Characteristics and properties of osteocytes in culture. J. Bone Miner. Res. **9:**1697–1704.
46. **Leupin O, Kramer I, Collette NM, Loots GG, Natt F, Kneissel M, Keller H.** 2007. Control of the SOST bone enhancer by PTH using MEF2 transcription factors. J. Bone Miner. Res. **22:**1957–1967. http://dx.doi.org/10.1359/jbmr.070804.
47. **Powell WF, Jr, Barry KJ, Tulum I, Kobayashi T, Harris SE, Bringhurst FR, Pajevic PD.** 2011. Targeted ablation of the PTH/PTHrP receptor in osteocytes impairs bone structure and homeostatic calcemic responses. J. Endocrinol. **209:**21–32. http://dx.doi.org/10.1530/JOE-10-0308.
48. **Saini V, Marengi DA, Barry KJ, Fulzele KS, Heiden E, Liu X, Dedic C, Maeda A, Lotinun S, Baron R, Pajevic PD.** 2013. Parathyroid hormone (PTH)/PTH-related peptide type 1 receptor (PPR) signaling in osteocytes regulates anabolic and catabolic skeletal responses to PTH. J. Biol. Chem. **288:**20122–20134. http://dx.doi.org/10.1074/jbc.M112.441360.
49. **Kato Y, Windle JJ, Koop BA, Mundy GR, Bonewald LF.** 1997. Establishment of an osteocyte-like cell line, MLO-Y4. J. Bone Miner. Res. **12:**2014–2023.
50. **Kao RS, Abbott MJ, Louie A, O'Carroll D, Lu W, Nissenson R.** 2013. Constitutive protein kinase A activity in osteocytes and late osteoblasts produces an anabolic effect on bone. Bone **55:**277–287. http://dx.doi.org/10.1016/j.bone.2013.04.001.
51. **O'Brien CA, Plotkin LI, Galli C, Goellner JJ, Gortazar AR, Allen MR, Robling AG, Bouxsein M, Schipani E, Turner CH, Jilka RL, Weinstein RS, Manolagas SC, Bellido T.** 2008. Control of bone mass and remodeling by PTH receptor signaling in osteocytes. PLoS One **3:**e2942. http://dx.doi.org/10.1371/journal.pone.0002942.
52. **Rhee Y, Allen MR, Condon K, Lezcano V, Ronda AC, Galli C, Olivos N, Passeri G, O'Brien CA, Bivi N, Plotkin LI, Bellido T.** 2011. PTH receptor signaling in osteocytes governs periosteal bone formation and intracortical remodeling. J. Bone Miner. Res. **26:**1035–1046. http://dx.doi.org/10.1002/jbmr.304.
53. **Hekmatnejad B, Akhouayri O, Jafarov T, St-Arnaud R.** 2013. Sumoylated alphaNAC potentiates transcriptional repression by fiat. J. Cell. Biochem. http://dx.doi.org/10.1002/jcb.24279.
54. **Quelo I, Akhouayri O, Prud'homme J, St-Arnaud R.** 2004. GSK3beta-dependent phosphorylation of the alphaNAC coactivator regulates its nuclear translocation and proteasome-mediated degradation. Biochemistry **43:**2906–2914. http://dx.doi.org/10.1021/bi036256+.
55. **Mak IW, Turcotte RE, Popovic S, Singh G, Ghert M.** 2011. AP-1 as a regulator of MMP-13 in the stromal cell of giant cell tumor of bone. Biochem. Res. Int. **2011:**164197. http://dx.doi.org/10.1155/2011/164197.
56. **Scott DK, Brakenhoff KD, Clohisy JC, Quinn CO, Partridge NC.** 1992. Parathyroid hormone induces transcription of collagenase in rat osteoblastic cells by a mechanism using cyclic adenosine 3′,5′-monophosphate and requiring protein synthesis. Mol. Endocrinol. **6:**2153–2159. http://dx.doi.org/10.1210/mend.6.12.1337147.
57. **Bouxsein ML, Boyd SK, Christiansen BA, Guldberg RE, Jepsen KJ, Muller R.** 2010. Guidelines for assessment of bone microstructure in rodents using micro-computed tomography. J. Bone Miner. Res. **25:**1468–1486. http://dx.doi.org/10.1002/jbmr.141.